The Astrophysical Journal Letters, 833:L20 (6pp), 2016 December 20 doi:10.3847/2041-8213/833/2/L20

THE RED SEQUENCE AT BIRTH IN THE GALAXY CLUSTER Cl J1449+0856 AT $z = 2$

V. Strazzullo[1], E. Daddi[2], R. Gobat[3], F. Valentino[2], M. Pannella[1], M. Dickinson[4], A. Renzini[5], G. Brammer[6], M. Onodera[7,8], A. Finoguenov[9,10], A. Cimatti[11], C. M. Carollo[12], and N. Arimoto[7,8]
[1] Department of Physics, Ludwig-Maximilians-Universität, Scheinerstr. 1, D-81679 München, Germany; vstrazz@usm.lmu.de
[2] Irfu/Service d'Astrophysique, CEA Saclay, Orme des Merisiers, F-91191 Gif sur Yvette, France
[3] School of Physics, Korea Institute for Advanced Study, Hoegiro 85, Dongdaemun-gu, Seoul 130-722, Korea
[4] National Optical Astronomy Observatory, 950 North Cherry Avenue, Tucson, AZ 85719, USA
[5] INAF-Osservatorio Astronomico di Padova, Vicolo dell'Osservatorio 5, I-35122, Padova, Italy
[6] Space Telescope Science Institute, 3700 San Martin Drive, Baltimore, MD 21218, USA
[7] Subaru Telescope, National Astronomical Observatory of Japan, National Institutes of Natural Sciences (NINS), 650 North A'ohoku Place, Hilo, HI, 96720, USA
[8] Department of Astronomical Science, SOKENDAI (The Graduate University for Advanced Studies), 650 North A'ohoku Place, Hilo, HI 96720, USA
[9] Max-Planck-Institut für extraterrestrische Physik, Giessenbachstrasse 1, D-85748 Garching, Germany
[10] Department of Physics, University of Helsinki, P.O. Box 64, FI-00014, Helsinki, Finland
[11] Dipartimento di Fisica e Astronomia, Universitá di Bologna, Viale Berti Pichat 6/2, I-30127, Bologna, Italy
[12] Institute for Astronomy, ETH Zürich, Wolfgang-Pauli-strasse 27, 8093 Zürich, Switzerland
Received 2016 October 29; revised 2016 November 21; accepted 2016 November 22; published 2016 December 13

ABSTRACT

We use *Hubble Space Telescope*/WFC3 imaging to study the red population in the IR-selected, X-ray detected, low-mass cluster Cl J1449+0856 at $z = 2$, one of the few bona fide established clusters discovered at this redshift, and likely a typical progenitor of an average massive cluster today. This study explores the presence and significance of an early red sequence in the core of this structure, investigating the nature of red-sequence galaxies, highlighting environmental effects on cluster galaxy populations at high redshift, and at the same time underlining similarities and differences with other distant dense environments. Our results suggest that the red population in the core of Cl J1449+0856 is made of a mixture of quiescent and dusty star-forming galaxies, with a seedling of the future red sequence already growing in the very central cluster region, and already characterizing the inner cluster core with respect to lower-density environments. On the other hand, the color–magnitude diagram of this cluster is definitely different from that of lower-redshift $z \lesssim 1$ clusters, as well as of some rare particularly evolved massive clusters at similar redshift, and it is suggestive of a transition phase between active star formation and passive evolution occurring in the protocluster and established lower-redshift cluster regimes.

Key words: galaxies: clusters: individual (Cl J1449+0856) – galaxies: evolution – galaxies: high-redshift

1. INTRODUCTION

In the nearby universe and up to $z \sim 1$, cluster cores host the most massive early-type galaxies containing stars nearly as old as the Hubble time, making for a red sequence in their color–magnitude diagram (CMD; e.g., Kodama & Arimoto 1997; Mei et al. 2009), often considered as a defining signature of dense environments. Observations of the evolution of the red galaxy population back to the protocluster regime show that, although massive passive galaxies and tight red sequences in cluster cores are already common even earlier than $z \sim 1$ (e.g., Lidman et al. 2008; Newman et al. 2014), the red sequence seems to increase its scatter, depopulate at lower stellar masses (note possible dependence on cluster mass; e.g., Tanaka et al. 2007; Andreon 2008; Hilton et al. 2009; Papovich et al. 2010; Lemaux et al. 2012; Rudnick et al. 2012; Cerulo et al. 2016) and eventually dissolve in most distant cluster progenitor environments. A first sequence probably appears at high stellar masses just before $z \sim 2$ (Kodama et al. 2007; Zirm et al. 2008), in agreement with star formation histories inferred for lower-redshift passive cluster galaxies (e.g., Gobat et al. 2008; Rettura et al. 2010; Strazzullo et al. 2010; Snyder et al. 2012), placing their major star formation epoch at $z_f \gtrsim 2$.

In the last few years, cluster studies systematically approached this expected formation epoch and indeed started revealing increasing star formation, nuclear, and merging activity in $z \gtrsim 1.5$ clusters (e.g., Hilton et al. 2010; Hayashi et al. 2011; Stanford et al. 2012; Brodwin et al. 2013; Santos et al. 2015; Tran et al. 2015; Webb et al. 2015; Alberts et al. 2016). Wang et al.'s (2016) study of a $z = 2.5$ structure seemingly captures the massive star formation event likely producing the future red sequence. On the other hand, although often co-existing with still actively star-forming (SF) sources, quiescent galaxies are found in cluster cores even up to $z \sim 2$ (e.g., Kurk et al. 2009; Gobat et al. 2011, 2013; Spitler et al. 2012; Strazzullo et al. 2013; Tanaka et al. 2013; Newman et al. 2014; Smail et al. 2014; Cooke et al. 2016), with enhanced quiescent fractions with respect to field levels testifying to an early onset of environmental signatures on galaxy population properties.

In this work, we follow up on our previous studies of the cluster Cl J1449+0856 (hereafter ClJ1449) at $z = 1.995$ (Gobat et al. 2011, 2013; Strazzullo et al. 2013; Valentino et al. 2015, 2016, hereafter G11, G13, S13, V15, V16, respectively) with an investigation of the CMD based on *Hubble Space Telescope* (*HST*) observations. These data provide a deep, high-resolution probe of the rest-frame $\sim U$–B color of galaxies in ClJ1449, significantly improving our previous photometric analyses and eventually enabling a study of the red population in one of the most distant cluster environments known thus far.

ClJ1449 is a low-mass ($\sim 5 \cdot 10^{13}\ M_{\odot}$), IRAC-color selected, X-ray detected structure in the mass range of typical progenitors of today's massive clusters (G11). In contrast with rare examples of impressively evolved structures at similar redshift (Andreon et al. 2014; Newman et al. 2014), ClJ1449

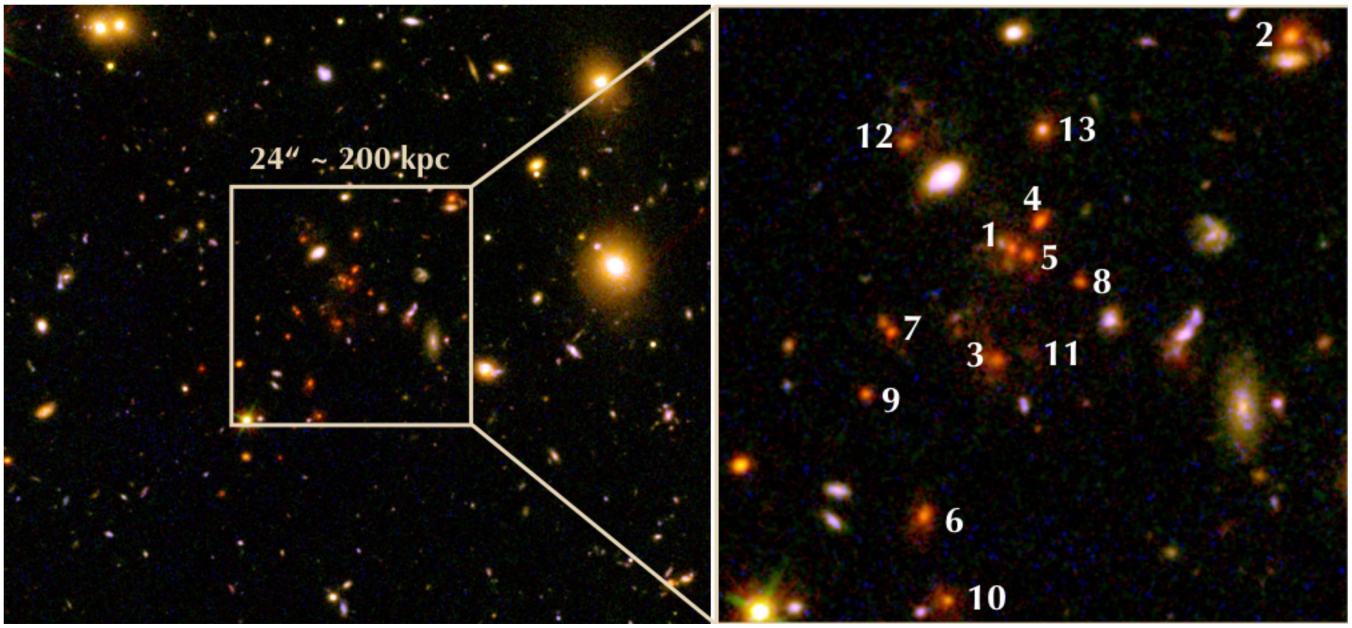

Figure 1. F606W-F105W-F140W pseudo-color image of ClJ1449 (left; $\sim 60'' \times 70''$), and a zoom into the cluster center (right; $\sim 200 \times 200$ kpc^2 (proper) at $z = 2$). In the right panel, numbers mark red sources discussed in this work.

thus probably draws a more common picture of galaxy populations in the first clusters at this crucial epoch.

We assume $\Omega_M = 0.3$, $\Omega_\Lambda = 0.7$, $H_0 = 70$ km s^{-1} Mpc^{-1}, and a Salpeter (1955) IMF. Magnitudes are in the AB system.

2. OBSERVATIONS AND MEASUREMENTS

This work is largely based on *HST* Wide Field Camera 3 (WFC3) observations of ClJ1449 in the F105W and F140W bands. Figure 1 shows an image of the cluster field and highlights all potential red cluster members in the central region (m105–m140 > 0.9, $r < 200$ kpc). We further use optical/NIR data and derived quantities from our previous work, and specifically spectroscopic redshifts (G11; G13; V15) to identify cluster members, complemented with photometric redshift (photo-z) based membership (S13; see original papers for details). In the following we refer to: (i) interlopers including spectroscopic and photo-z interlopers; (ii) possible members including uncertain, low-likelihood photo-z candidate members (S13); and (iii) members including spectroscopic and high-likelihood photo-z members (S13). We use photometric measurements and derived quantities from S13, complemented where needed with new measurements performed with the same approach accounting for the new F105W data.[13]

We also use a control field of ~ 60 arcmin^2 in the CANDELS (Grogin et al. 2011) GOODS-S field as a statistical comparison for galaxy populations in ClJ1449. We use multiwavelength photometry from Guo et al. (2013) and photo-zs from Schreiber et al. (2015). Lacking sufficiently deep F140W-band imaging, we measure synthetic m140 magnitudes by convolving best-fit SEDs from Pannella et al. (2015) with the F140W response function. In the magnitude range of interest, we estimate a $\lesssim 0.1$ mag uncertainty for these synthetic magnitudes, which is not relevant for our purposes.

3. THE COLOR–MAGNITUDE DIAGRAM

Figure 2(a) shows the F105W-F140W CMD in the field of ClJ1449, over a region extending to a maximum clustercentric distance $r = 500$ kpc (proper) at $z = 2$ ($\sim 1'$, about the estimated $r_{200} \sim 0.'78 \sim 0.4 \pm 0.1$ Mpc for ClJ1449; G13; V16). All galaxies in the probed field are shown, but cluster members are highlighted with colored symbols according to their stellar population properties (Section 4; Figure 5).

Figure 2(c) shows an alternative, photo-z independent picture of the CMD, largely based on statistical background subtraction (individual membership is only considered for spectroscopic sources and only affects Figure 2(c) in minor details). This CMD is obtained by subtracting, for each galaxy in the control (GOODS-S) field, an area-normalized fractional galaxy contribution to the closest galaxy in color–magnitude space in the ClJ1449 field (see, e.g., van der Burg et al. 2016). All galaxies in the ClJ1449 field are shown (black/gray and colored symbols for the full field and $r < 150$ kpc CMD, respectively), but symbol size/color scales with their excess probability over the control field CMD. The excess probability[14] across the CMD of Figure 2(c) is meant to represent the background-subtracted color–magnitude distribution of cluster galaxies in ClJ1449, as an independent confirmation of the color distribution based on individual membership shown in Figure 2(a).

As compared with $z \lesssim 1$ clusters, or even with the massive $z = 1.8$ cluster JKCS041 (Newman et al. 2014), the CMD of ClJ1449 shows a clearly less dominant, more scattered red galaxy population. Nonetheless, a first albeit still sparsely populated red sequence is found close to the expected location,

[13] Measurements for some galaxies will thus differ from those in S13. We note (in particular for source ID 1; see Figure 1) that the new F105W data support in some (rare) cases a different source extraction than the one used in S13, resulting in different source properties. Furthermore, we redetermined stellar masses using the newly available photometry, and—in contrast to S13—using the original photometric zero-points rather than those adjusted for photo-z determination. Stellar masses used here are thus not identical to those in S13.

[14] Being *statistical*, the excess probability in Figure 2(c) obviously does not directly reflect cluster membership probability on a galaxy-by-galaxy basis.

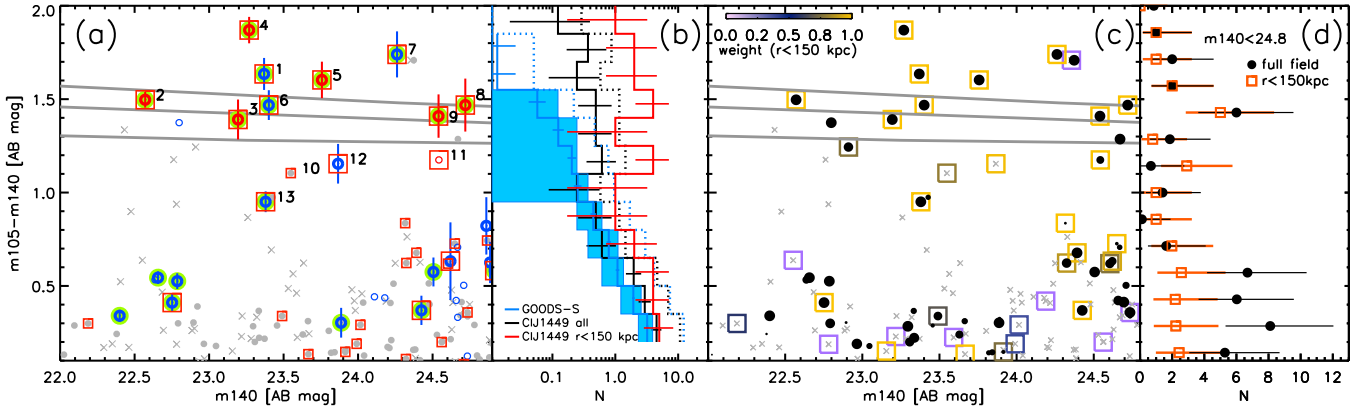

Figure 2. Panel (a): CMD of all galaxies in the ClJ1449 field (F140W MAG_AUTO vs. F105W-F140W aperture color, 0.″6 diameter). Thick colored symbols show cluster members; spectroscopic members are highlighted with green shading. Low-likelihood candidate members are shown with small colored symbols, and photometric and spectroscopic interlopers with gray points and crosses, respectively. Color-coding of members reflects the classification from Figure 5 (see the text). Red squares mark all galaxies (but spectroscopic interlopers) within 150 kpc from the cluster center. Red sources are numbered as in Figure 1. The three gray lines show the KA97 model red sequence at $z = 2$ for $z_f = 3$, 5, 10. Panel (b): the color histogram of *all* $22 < m140 < 24.8$ galaxies in the ClJ1449 field (black, solid), within $r < 150$ kpc from the cluster center (red), and in the GOODS-S control field (blue, solid), all normalized to the projected area within $r < 150$ kpc. The cyan-shaded area around the blue line shows an estimate of cosmic variance from cluster field-sized apertures randomly placed over the control field. Dotted lines show histograms normalized to the total number of galaxies within $r < 150$ kpc. Panel (c): a visual rendition of the CMD based on statistical background subtraction (see the text). Black points show *all* galaxies in the ClJ1449 field, with symbol size scaling with their excess probability over the CMD in the control field (galaxies with zero excess probability are plotted as gray crosses—see the text for details). Colored squares show this statistically background-subtracted CMD in the central $r < 150$ kpc; symbol color scales with excess probability according to the upper left color bar. Panel (d): the statistically background-subtracted (from panel (c) color distribution of cluster galaxies, in the full ClJ1449 field and within $r < 150$ kpc.

confirming the presence of a characteristic population of red sources in the cluster core (G11; G13; S13), and further highlighting red-sequence outliers. As a reference, the red sequence predicted at $z = 2$ by Kodama & Arimoto (1997, KA97) models is also shown. An estimate of the intrinsic m105–m140 scatter (rest-frame $\sim U$–B; determined as in Lidman et al. 2008, in our case affected by very poor statistics) of *all* core ($r < 150$ kpc) red members with m105–m140 > 1.2 (regardless of their quiescent/SF nature; see Section 4) is $\sigma_{\rm int} = 0.14^{+0.03}_{-0.07}$ ($\sigma_{\rm int} = 0.12 \pm 0.03$ if considering only core members consistent within 0.15 mag with the KA97 $3 < z_f < 10$ models). On the other hand, with the exception of ID 4 *quiescent* members lie on a tight sequence with $z_f \gtrsim 5$ (see Sections 4, 5; see also, e.g., Stanford et al. 2012).

Figures 2(b) and (d) show, respectively, the color distribution of *all* $22 < m140 < 24.8$ galaxies in the ClJ1449 field (full field and $r < 150$ kpc) and of *cluster* galaxies (statistically background subtracted as from Figure 2(c)). Figure 2(b) also shows for comparison the color distribution of *all* $22 < m140 < 24.8$ galaxies in the control field. Figures 2(b) and (d) are not affected by uncertainties in the individual membership determination, as they use the full galaxy sample or a statistically background-subtracted sample (as for Figure 2(c)). They thus provide further confirmation and quantification of the excess population of red sources in the cluster field shown in Figure 2(a).

Besides the very clear excess of red galaxies, Figure 2 generally suggests that the "green valley" is still indeed an underdense region in the CMD of ClJ1449 over the full ($r < 500$ kpc) area probed, with the excess of red sources being located at markedly redder colors, thus constraining the relevance of the population transitioning from the "blue cloud" at bright magnitudes. On the other hand, although statistics are very poor, we note that virtually all green-valley sources likely belonging to the cluster are located within $r < 150$ kpc from the cluster center.

4. THE RED POPULATION

In order to further highlight the relevance of the red population in ClJ1449, Figure 3 compares the F140W luminosity functions (LFs) of all and red galaxies in the ClJ1449 field and in the central $r < 150$ kpc area. The LF is essentially determined through statistical background subtraction using the GOODS-S control field (though we make use of spectroscopic and photometric redshift information to remove obvious interlopers, in particular at the bright end where statistics are very poor; e.g., Strazzullo et al. 2010). The "red" galaxy LF is obtained selecting galaxies with m105–m140 > 1.1 and, here again, includes the full red population regardless of stellar population properties discussed below. Figure 3 also shows the corresponding red fraction as a function of m140 magnitude, determined as the ratio of the red and the total LFs, and compared with the analogous red fraction for $1.7 < z_{\rm phot} < 2.3$ galaxies in the GOODS-S control field. Like Figure 2, Figure 3 shows again that the red population is enhanced only in the very central cluster region, the red fraction in the overall cluster virial volume is similar to the control field levels.

Finally, Figure 4 shows the color-stellar mass diagram for cluster members, highlighting that, as expected, optically blue galaxies are typically restricted to low stellar masses, while the high-mass population is typically dominated by red sources (old or dusty; see Section 4 below).

The actual nature of the red population shown in Figure 2 deserves further discussion. Sources labeled as IDs 1, 4, and 5 in Figure 2(a) are part of what G11 identified as a "proto-BCG" still in active formation (see Figure 1, right). The high-resolution deep *HST* imaging, as well as ALMA observations (V. Strazzullo et al. 2016, in preparation), indeed reveal a complex structure with multiple components. According to photometric and spectroscopic analysis, S13 and G13 classified IDs 1 and 4 of this proto-BCG complex as (dusty) SF and quiescent, respectively; IDs 2, 3, 6, 8, and 9 were also classified as quiescent. The sample of "red sources" highlighted in

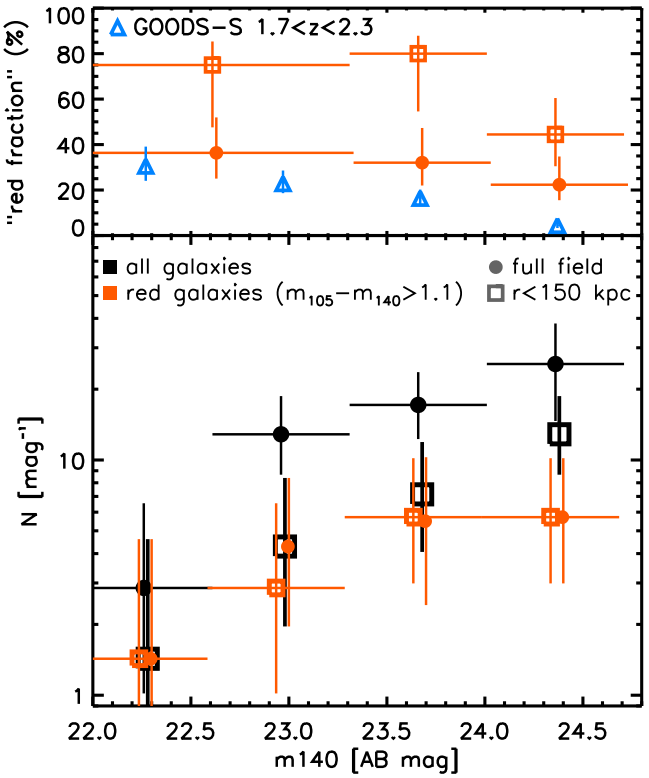

Figure 3. Bottom panel: the F140W LF in the field of ClJ1449. Filled circles and empty squares show the LF in the full field and within $r < 150$ kpc. Black and red symbols refer to the full sample and to red galaxies, respectively (see the text for details). Error bars show Poisson errors. Top panel: red points show the red fraction in ClJ1449 from the ratio of the red and total LFs in the bottom panel. Blue points show the corresponding red fraction in the GOODS-S control field for galaxies at $1.7 < z < 2.3$. Errors are calculated following Cameron et al. (2011).

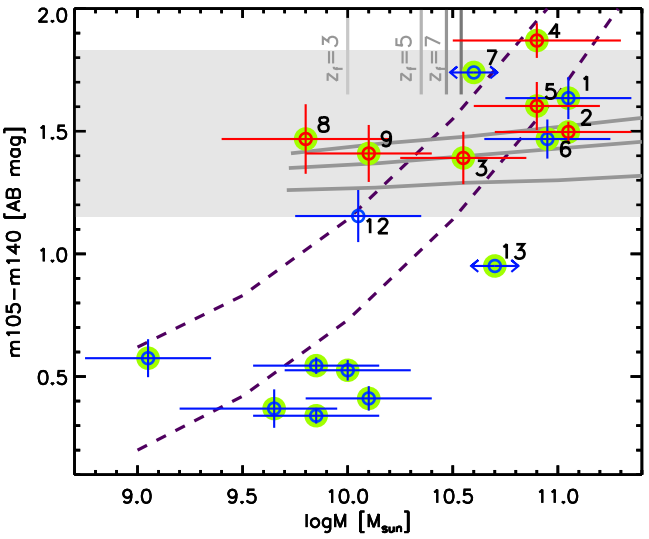

Figure 4. Color-mass diagram of cluster members in the magnitude range $22 <$ m140 < 24.7 (see Figure 2). Color-coding follows Figure 2. Vertical gray lines show the stellar mass of a m140 = 24.7, solar-metallicity BC03 SSP with different formation redshifts: the darkest line corresponds to a maximally old population, approximately marking the mass completeness of the sample for passive dust-free galaxies. The gray area shows the color range of passive BC03 SSPs from Figure 5. Gray slanted lines show KA97 models from Figure 2. Dashed purple lines show, as a reference, constant-SFR BC03 models of age = 0.1, 1 Gyr, affected by mass-dependent dust reddening as from Pannella et al. (2015).

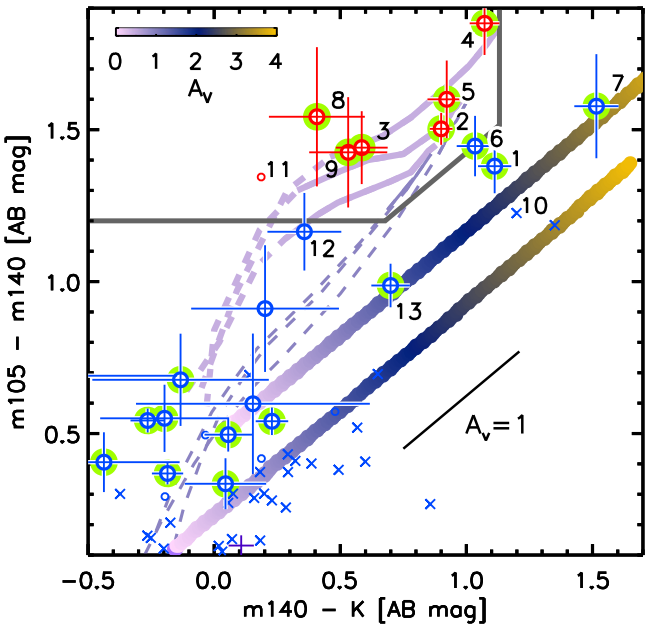

Figure 5. The m105–m140 vs. m140-K plot for cluster members (symbol coding as in Figure 2; photo-z interlopers are still shown as crosses). The thick colored lines show for reference the colors of two BC03 constant-SFR models at $z = 2$, with ages 0.1 and 1 Gyr, and dust attenuation according to the top left color scale. Thin purple lines show the age evolution of models with $\tau = 0$ and 0.5 Gyr, $0.008 < Z < 0.05$, and $A_V = 0$; lines are dashed until age > 0.5 Gyr and age$/\tau > 4$, then become solid lines (see the text). The gray line defines the adopted region of "passive galaxies" (upper left part of the plot), determining the color-coding of points: red/blue for galaxies in the passive/star-forming regions, respectively.

Figure 1 further includes four green-valley sources, IDs 10 to 13; based on photo-zs, IDs 10 and 11 are probably interlopers.

We note that IDs 7 and 13 are AGN hosts (G13); that may affect their colors and derived properties (together with significant neighbor contamination of ground-based and IRAC photometry for ID 7). Although we include them for completeness in the figures, a proper analysis of the nature of these two sources is postponed to future work, and we thus do not consider them further in the following discussion.

The new F105W imaging allows a further photometric classification of galaxy stellar populations, similar in principle to the UVJ or p/sBzK approaches (Daddi et al. 2004; Williams et al. 2009) aiming at a separation of quiescent and SF galaxies accounting for dust reddening, and independent of SED modeling (as we used in S13), which may be particularly affected by blending in the crowded cluster center when using imaging with poorer resolution. Figure 5 shows the m140-K versus m105–m140 color–color plot for cluster members (1″ diameter aperture colors).[15]

We consider the position of cluster galaxies in this diagram to constrain the nature of their stellar populations. As an indicative reference of the location of SF populations in this diagram, we show the colors of two constant star formation rate (SFR) BC03 models at $z = 2$ with ages 0.1 and 1 Gyr, attenuated according to Calzetti et al. (2000) with $0 < A_V < 4$. The evolution of (dust-free) models with $\tau = 0$ (SSP) and

[15] Because of the combination with ground-based K-band imaging, this aperture is larger than the one used in Figure 2. Although color gradients between these two apertures are generally small, there are few exceptions, notably IDs 1 and 7; given the complex surroundings of these sources this might be partly due to contamination by other sources/components.

0.5 Gyr, and $0.008 < Z < 0.05$, is also shown, for ages up to the age of the universe at $z = 2$. As Figure 5 shows, this *observed* color combination still allows for the definition of a quiescent region with a boundary parallel to the reddening vector, enabling a classification of stellar populations only relying on observed magnitudes from imaging with relatively good resolution.

For the vast majority of sources, the quiescent/SF classification from Figure 5 agrees with that UVJ/SED-based from S13. The notable exception relevant for this work is ID 6 (and partly ID13 with an uncertain classification in S13). In Figure 5, IDs 1, 6, and 12 are formally in the SF region, although very close to the boundary line, thus their m105–m140-K classification may be deemed uncertain. However, the recently identified ALMA continuum and CO(4-3) emission from ID 6 supports its dusty SF nature. Concerning ID 1, as discussed in G11, *Spitzer*/MIPS 24 μm emission was observed close to the location of the proto-BCG. However, the ALMA-detected 870 μm continuum and CO(4-3) emission is clearly associated with a very red faint component south of the main bright sources discussed here, IDs 1, 4, 5, which are instead all below the 870 μm map 2σ level (0.2 mJy, $\sim 40\, M_{\odot}\, \mathrm{yr}^{-1}$; e.g., Béthermin et al. 2012), as all other red and green-valley sources discussed here besides ID 6. Given the estimated stellar masses and colors, this may suggest that most of the massive red sources IDs 1, 2, 3, 4, 5 are likely quiescent/suppressed-SF (at least with respect to the expected mass–SFR relation; e.g., Elbaz et al. 2011) rather than dusty massively SF galaxies. We recall nonetheless the significant uncertainties inherent to this kind of analysis; a more detailed discussion of the ALMA observations will be presented in V. Strazzullo et al. (2016, in preparation). For IDs 8, 9, 12, 13, given the expected stellar masses and SFRs, the available ALMA observations do not add significant constraints.

5. CONCLUSIONS

We use *HST*/WFC3 observations to further investigate the population of optically red galaxies in the cluster ClJ1449 at $z = 2$. This work highlights once more the presence of a numerically small but characteristic population of red galaxies concentrated within $r < 150$ kpc from the cluster center. Many of these red sources lie along a "red sequence" that is close to passive evolution expectations at this redshift; however, this sequence is significantly more scattered than in $z \lesssim 1$ clusters (e.g., Mei et al. 2009; Foltz et al. 2015), notably with the presence of extremely red sources, and is partly contaminated by dusty SF galaxies. The red population in ClJ1449 is more sparse and scattered even as compared with some (rather exceptional) cluster at similar redshift (notably JKCS041 at $z = 1.8$; Newman et al. 2014), although we also note results from, e.g., Hilton et al. (2010), Papovich et al. (2010), Stanford et al. (2012), Cerulo et al. (2016), and references therein, on the marked increase of cluster red-sequence scatter at $z \gtrsim 1.4$.

Even among the red galaxies that are deemed to be quiescent rather than dusty SF, two sources scatter above the KA07 $z_f \sim 10$ red-sequence prediction (IDs 4 and 5), suggesting dust attenuation and/or supersolar metallicity (see Figure 5), although we recall the especially crowded environment of these specific galaxies possibly affecting photometric accuracy. As a reference, the colors of ID 4 may be reproduced with a young (age $\sim$0.5 to $\sim$1 Gyr) solar-metallicity BC03 SSP with $A_V \sim 1.5$–1, or possibly with a dust-free supersolar ($Z = 0.05$) SSP with a $z_f \gtrsim 6$.

Early and recent results on the investigation of optically red galaxies in dense environments at $z \gtrsim 2$ highlighted the—sometimes dominant—contribution of dusty, highly SF sources (e.g., Zirm et al. 2008; Wang et al. 2016). The analysis presented here, also with the support of recent ALMA observations, suggests that indeed ClJ1449 hosts in its very central region a mixture of quiescent and dusty SF galaxies, at the same time highlighting a population that is seemingly dominated in number by galaxies with suppressed star formation making for a first, still forming red-sequence seedling. In combination with previous work, this study underlines differences and similarities in galaxy population properties of cluster progenitors of different masses in a crucial redshift range, providing the picture of one of the most distant spectroscopically confirmed bona fide cluster environments with an estimated mass placing it among the average progenitors of today's clusters rather than exceptionally massive structures.

V.S., E.D., R.G., and F.V. were supported by grants ERC-StG UPGAL 240039 and ANR-08-JCJC-0008. Based on observations from *HST* programs GO-11648 and GO-12991.

REFERENCES

Alberts, S., Pope, A., Brodwin, M., et al. 2016, ApJ, 825, 72
Andreon, S. 2008, MNRAS, 386, 1045
Andreon, S., Newman, A. B., Trinchieri, G., et al. 2014, A&A, 565, A120
Béthermin, M., Daddi, E., Magdis, G., et al. 2012, ApJL, 757, L23
Brodwin, M., Stanford, S. A., Gonzalez, A. H., et al. 2013, ApJ, 779, 138
Calzetti, D., Armus, L., Bohlin, R. C., et al. 2000, ApJ, 533, 682
Cameron, E., Carollo, C. M., Oesch, P. A., et al. 2011, ApJ, 743, 146
Cerulo, P., Couch, W. J., Lidman, C., et al. 2016, MNRAS, 457, 2209
Cooke, E. A., Hatch, N. A., Stern, D., et al. 2016, ApJ, 816, 83
Daddi, E., Cimatti, A., Renzini, A., et al. 2004, ApJ, 617, 746
Elbaz, D., Dickinson, M., Hwang, H. S., et al. 2011, A&A, 533, A119
Foltz, R., Rettura, A., Wilson, G., et al. 2015, ApJ, 812, 138
Gobat, R., Daddi, E., Onodera, M., et al. 2011, A&A, 526, A133
Gobat, R., Rosati, P., Strazzullo, V., et al. 2008, A&A, 488, 853
Gobat, R., Strazzullo, V., Daddi, E., et al. 2013, ApJ, 776, 9
Grogin, N. A., Kocevski, D. D., Faber, S. M., et al. 2011, ApJS, 197, 35
Guo, Y., Ferguson, H. C., Giavalisco, M., et al. 2013, ApJS, 207, 24
Hayashi, M., Kodama, T., Koyama, Y., Tadaki, K.-I., & Tanaka, I. 2011, MNRAS, 415, 2670
Hilton, M., Lloyd-Davies, E., Stanford, S. A., et al. 2010, ApJ, 718, 133
Hilton, M., Stanford, S. A., Stott, J. P., et al. 2009, ApJ, 697, 436
Kodama, T., & Arimoto, N. 1997, A&A, 320, 41
Kodama, T., Tanaka, I., Kajisawa, M., et al. 2007, MNRAS, 377, 1717
Kurk, J., Cimatti, A., Zamorani, G., et al. 2009, A&A, 504, 331
Lemaux, B. C., Gal, R. R., Lubin, L. M., et al. 2012, ApJ, 745, 106
Lidman, C., Rosati, P., Tanaka, M., et al. 2008, A&A, 489, 981
Mei, S., Holden, B. P., Blakeslee, J. P., et al. 2009, ApJ, 690, 42
Newman, A. B., Ellis, R. S., Andreon, S., et al. 2014, ApJ, 788, 51
Pannella, M., Elbaz, D., Daddi, E., et al. 2015, ApJ, 807, 141
Papovich, C., Momcheva, I., Willmer, C. N. A., et al. 2010, ApJ, 716, 1503
Rettura, A., Rosati, P., Nonino, M., et al. 2010, ApJ, 709, 512
Rudnick, G. H., Tran, K.-V., Papovich, C., Momcheva, I., & Willmer, C. 2012, ApJ, 755, 14
Salpeter, E. E. 1955, ApJ, 121, 161
Santos, J. S., Altieri, B., Valtchanov, I., et al. 2015, MNRAS, 447, L65
Schreiber, C., Pannella, M., Elbaz, D., et al. 2015, A&A, 575, A74
Smail, I., Geach, J. E., Swinbank, A. M., et al. 2014, ApJ, 782, 19
Snyder, G. F., Brodwin, M., Mancone, C. M., et al. 2012, ApJ, 756, 114
Spitler, L. R., Labbé, I., Glazebrook, K., et al. 2012, ApJL, 748, L21
Stanford, S. A., Brodwin, M., Gonzalez, A. H., et al. 2012, ApJ, 753, 164
Strazzullo, V., Gobat, R., Daddi, E., et al. 2013, ApJ, 772, 118
Strazzullo, V., Rosati, P., Pannella, M., et al. 2010, A&A, 524, A17
Tanaka, M., Kodama, T., Kajisawa, M., et al. 2007, MNRAS, 377, 1206
Tanaka, M., Toft, S., Marchesini, D., et al. 2013, ApJ, 772, 113

Tran, K.-V. H., Nanayakkara, T., Yuan, T., et al. 2015, ApJ, 811, 28
Valentino, F., Daddi, E., Finoguenov, A., et al. 2016, ApJ, 829, 53
Valentino, F., Daddi, E., Strazzullo, V., et al. 2015, ApJ, 801, 132
van der Burg, R. F. J., Muzzin, A., & Hoekstra, H. 2016, A&A, 590, A20
Wang, T., Elbaz, D., Daddi, E., et al. 2016, ApJ, 828, 56
Webb, T., Noble, A., DeGroot, A., et al. 2015, ApJ, 809, 173
Williams, R. J., Quadri, R. F., Franx, M., et al. 2009, ApJ, 691, 1879
Zirm, A. W., Stanford, S. A., Postman, M., et al. 2008, ApJ, 680, 224